UNIVERSIDADE DE BRASÍLIA – UNB

FACULDADE DE CIÊNCIAS E TECNOLOGIAS DA ENGENHARIA

PROGRAMA DE PÓS-GRADUAÇÃO EM INTEGRIDADE DE MATERIAIS DA ENGENHARIA

COMPARISON OF THE PERFORMANCE AND DYNAMICS OF A CYLINDRICAL HALL THRUSTER WITH DIFFERENT INPUT POWER VIA NUMERICAL SIMULATIONS

SERGIO THADEU TAVARES DA SILVA JUNIOR

ADVISOR: PROF. DR. RODRIGO ANDRES MIRANDA CERDA

UNIVERSIDADE DE BRASÍLIA – UNB
FACULDADE DE CIÊNCIAS E TECNOLOGIAS DA ENGENHARIA

COMPARISON OF THE PERFORMANCE AND DYNAMICS OF A CYLINDRICAL HALL THRUSTER WITH DIFFERENT INPUT POWER VIA NUMERICAL SIMULATIONS

SERGIO THADEU TAVARES DA SILVA JUNIOR

ADVISOR: PROF. DR. RODRIGO ANDRES MIRANDA CERDA

MASTER THESIS IN INTEGRITY OF MATERIALS ENGINEERING
ISSUE: 112A/2024

BRASÍLIA/DF, DECEMBER 2024

UNIVERSIDADE DE BRASÍLIA – UNB
FACULDADE DE CIÊNCIAS E TECNOLOGIAS DA ENGENHARIA
PROGRAMA DE PÓS-GRADUAÇÃO EM INTEGRIDADE DE MATERIAIS DA ENGENHARIA

COMPARISON OF THE PERFORMANCE AND DYNAMICS OF A CYLINDRICAL HALL THRUSTER WITH DIFFERENT INPUT POWER VIA NUMERICAL SIMULATIONS

SERGIO THADEU TAVARES DA SILVA JUNIOR

MASTER'S THESIS SUBMITTED TO THE POSTGRADUATE PROGRAM IN INTEGRITY OF MATERIALS ENGINEERING AT UNIVERSITY OF BRASILIA, AS PART OF THE REQUIREMENTS FOR OBTAINING A MASTER'S DEGREE.

APPROVED BY:

PROF. DR. RODRIGO ANDRES MIRANDA CERDA
ADVISORR

DR. LUI TXAI CALVOSO HABL
EXAMINER - FCTE/UNIVERSITY OF BRASILIA

DR. JEAN CARLO SANTOS
EXAMINER - FACULTY/FEDERAL UNIVERSITY OF TECHNOLOGY OF PARANÁ

Relatório (ata) de defesa de dissertação assinado eletronicamente pela banca avaliadora, via Sistema Eletrônico de Informações - SEI, documento nº 12155009, processo nº 23106.113496/2024-83.

BRASÍLIA/DF, DECEMBER 2024

CATALOGRAPHIC CARD

JUNIOR, SERGIO
COMPARISON OF THE PERFORMANCE AND DYNAMICS OF A CYLINDRICAL HALL THRUSTER WITH DIFFERENT INPUT POWER VIA NUMERICAL SIMULATIONS
[Distrito Federal], 2024.
35p., 210 $\times$ 297 mm (FCTE - Faculdade de Ciências e Tecnologias da Engenharia,
Master in Integrity of Materials Engineering, 2024).
Master Thesis - University of Brasilia.
Faculdade de Ciências e Tecnologias da Engenharia

1. CubeSats	2. Electric Propulsion
3. Plasma	4. Ions
I. FCTE/UnB.	II. Title (series)

REFERENCE

JUNIOR, SERGIO (2024). COMPARISON OF THE PERFORMANCE AND DYNAMICS OF A CYLINDRICAL HALL THRUSTER WITH DIFFERENT INPUT POWER VIA NUMERICAL SIMULATIONS. Master's Thesis in Integrity of Engineering Materials, Publication 112A/2024, Postgraduate Program, Faculty of Engineering Sciences and Technologies, University of Brasília, Brasília, DF, 35p.

ASSIGNMENT OF RIGHTS

AUTHOR: Sergio Thadeu Tavares da Silva Junior

TITLE: COMPARISON OF THE PERFORMANCE AND DYNAMICS OF A CYLINDRICAL HALL THRUSTER WITH DIFFERENT INPUT POWER VIA NUMERICAL SIMULATIONS

DEGREE: Master

YEAR: 2024

sergiojunior@unb.br

Brasília, DF – Brazil

ACKNOWLEDGEMENTS

Agradeço primeiramente a Deus, que sempre iluminou meus caminhos e me deu força para superar os desafios dessa jornada. Aos meus avós, que representam a base de minha formação. Em especial, ao meu avô Tavares, cuja confiança nos meus estudos foi sempre fonte de motivação e a minha avó Lucy por seu carinho e dedicação inigualáveis.

Aos meus pais, Sérgio e Alcimara, meu agradecimento eterno por todo amor, apoio e pelos valores que me transmitiram, sendo exemplos de força, determinação e bondade que guiaram minha vida.

A minha esposa Gabrielle, pelo amor, compreensão e parceria em todos os momentos, e à sua família, por me acolherem com carinho. Ao professor Rodrigo Andres Miranda Cerda, agradeço pela paciência, orientação e confiança no meu potencial ao longo desta caminhada.

A cada um de vocês, meu mais sincero obrigado por tornarem esta conquista possível.

RESUMO

Comparação do desempenho e da dinâmica de um propulsor Hall cilíndrico com diferentes potenciais de entrada por meio de simulações numéricas.

Propulsão a plasma, ou propulsão elétrica, surge da necessidade de explorar o espaço profundo de forma mais econômica e eficiente. O Propulsor Hall Cilíndrico (CHT, do inglês Cylindrical Hall Thruster) demonstra uma utilização aprimorada do propelente e eficiências de desempenho dentro de dimensões reduzidas e limiares de potência mais baixos quando comparado aos aparelhos de propulsão a plasma convencionais. O tamanho compacto e a operação em níveis de potência mais baixos fazem dele uma opção interessante para fornecer propulsão para CubeSats e pequenos satélites. O CHT é composto por um canal com um ânodo anular através do qual o gás neutro é injetado e, posteriormente, ionizado por elétrons magnetizados injetados a partir de um cátodo oco externo. Os íons de plasma resultantes são ejetados do dispositivo, gerando impulso. Este trabalho visa compreender e estudar o plasma no canal de descarga de um CHT por meio de simulações numéricas. O código descreve o plasma com um modelo híbrido no qual os elétrons são tratados como um fluido e os íons e átomos neutros como pseudo-partículas. As simulações foram conduzidas para dois valores diferentes de potencial no ânodo, especificamente 150 V e 300 V, representando diferentes modos de operação. Os resultados obtidos com este modelo simplificado permitem obter uma configuração ideal para um futuro protótipo a ser implementado no Laboratório de Física de Plasma da Universidade de Brasília.

Palavras-chave: Cubesats, Propulsão Elétrica, Plasma, Ions.

ABSTRACT

Plasma propulsion, or electric propulsion, arises from the need to explore deep space more economically and efficiently. The Cylindrical Hall Thruster (CHT) demonstrates enhanced propellant utilization and performance efficiencies within reduced dimensions and lower power thresholds when compared to conventional plasma propulsion apparatuses. The compact size and operation at lower power levels make it an interesting option to provide propulsion for CubeSats and small satellites. The CHT comprises a channel with an annular anode through which neutral gas is injected, subsequently ionized by magnetized electrons injected from an external hollow cathode. The resulting plasma ions are ejected from the device, giving thrust. This work aims to understand and study the plasma in the discharge channel of a CHT through numerical simulations. The code describes the plasma with a hybrid model in which the electrons are treated as a fluid and the ions and neutral atoms as pseudo particles. The simulations were conducted for two different potential values at the anode, specifically 150 V and 300 V, representing different modes of operation. The results obtained with this simplified model allow to obtain an optimal configuration for a future prototype to be implemented at the Plasma Physics Laboratory at the University of Brasilia.

Keywords: CubeSats, Electric Propulsion, Plasma, Ions.

Contents

List of Tables

List of Figures

1 INTRODUCTION

The search for new technologies aimed at efficiently exploring deep space has been increasingly studied. The aerospace industry has, for the most part, used chemical propulsion, which provides a high amount of energy and a thrust sufficiently capable of overcoming the drag and weight forces, thus allowing space equipment to reach Earth orbit and even other planets (Goebel, 2008). However, one limitation of this type of propulsion is that, in order to launch a certain device, a high cost of fuel and oxidizer is necessary, in addition to significant storage space. These factors not only drive up expenses but also hinder the further advancement of space programs, impeding the realization of ambitious exploration objectives (Goebel, 2008).

Electric propulsion emerged as a promising alternative in the mid-1950s (Goebel, 2008). Hall Thrusters (HTs) are electric propulsion devices, depending on the $\mathbf{E} \times \mathbf{B}$ effect, where **E** represents the electric field and **B** the magnetic field, resulting in a current known as the Hall current. Hall thrusters are capable of accelerating ions to high speeds (Goebel, 2008). The particles that are accelerated are light and the impulse is on the order of mili-newtons (mN).

The Cylindrical Hall Thruster (CHT) represents an alternative HT design that comprises a cylindrical region and a short annular channel. The CHT demonstrates improved propellant utilization and performance when compared to HTs. The magnetic field can be adjusted using electromagnet coils or permanent magnets. This device has applicability for micro and nanosatellites because this device can offer a higher ionization efficiency , offering a better volume-to-surface ratio compared to compact HTs, potentially mitigating wall erosion (Raitses e Fisch, 2001; Miranda *et al.*, 2017).

The operation of CHT occurs by first filling a cylindrical chamber with neutral gas, with a small ring-shaped annular region near the surface of the anode. The non-magnetized ions are accelerated in the cylindrical channel by an electric field generated by the anode. Previous studies on the structure of this geometry assert that CHTs reduce the interaction between the plasma and the dielectric wall channel, electron transport, heat, and wall erosion (Seo *et al.*, 2013).

In this work we perform numerical simulations of a hybrid model of a cylindrical Hall thruster. We compare the performance of this thruster using two different values of the anode potential, namely, 150 V and 300 V. This work is organized as follows: Section 2 describes the objectives employed in this work; Section 3 shows plasma physics concepts relevant to apply to operation of the CHT; Section 4 contains the methodology that was used in this work;

while section 5 presents the simulation results, compare some kind of aspects such as thrust, efficiency and others; finally, section 6 resumes the findings and suggests future research directions.

2 OBJECTIVES

2.1 MAIN OBJECTIVE

Analyze the performance of a Cylindrical Hall Thruster (CHT) under different anode potential conditions through numerical simulations. The study aims to understand the plasma behavior, magnetic field interactions into the thruster and determine optimal configurations for CubeSats and small satellite applications.

2.2 SPECIFIC OBJECTIVES

- Conduct numerical simulations to map the magnetic field generated by permanent magnets in the Cylindrical Hall Thruster (CHT) using FEMM software.
- Use HALLIS software to study plasma dynamics in the CHT under two different anode potential values (150 V and 300 V).
- Compare performance parameters such as thrust, specific impulse, and efficiency between the simulated scenarios for the different potential values.
- Verify plasma density distribution, electrostatic potential and electron energy profiles in the discharge channel.
- Propose improvements for the development of future prototypes, focusing on feasibility and efficiency, to be implemented at the Plasma Physics Laboratory at the University of Brasília.

3 LITERATURE REVIEW

3.1 ELECTRIC PROPULSION

3.1.1 History

Electric propulsion began its development in the mid-1950s, as reported by Edgard Choueiri, who published the first detailed studies on this technology (Goebel, 2008). However, the initial concepts can be traced back to 1906 with Robert Goddard, who envisioned the possibility of non-chemical propellants. More robust research programs began in the 1960s with initiatives led by NASA (Choueiri, 2003).

Chemical propulsion, which has dominated the aerospace industry, relies on large quantities of fuel and oxidizer to generate the thrust necessary to overcome drag and weight forces, enabling spacecraft to reach Earth orbit and even other planets (Goebel, 2008). However, the high costs and storage requirements of this technology pose challenges to the development of more accessible and complex space programs. It was within this context that electric propulsion emerged as an alternative solution, offering greater efficiency and feasibility for long-duration missions and deep space exploration.

The first time an ion thruster was experimentally launched into Earth orbit was in the early sixties by the United States in conjunction with Russia. This experimental device used cesium and mercury as propellants. These tests continued until the mid-1980s (Goebel, 2008).

Russia began extensive use of electric propulsion, with Hall thrusters to keep communications satellites in orbit. Then in 1995, Japan launches its first ion system thruster (Goebel, 2008).The commercial use of this type of propulsion in the United States began in 1997 with the launch of the Xenon Ion Propulsion System (XIPS) (Goebel, 2008).

Plasma is considered the fourth state of matter and has had excellent applicability in the aerospace industry, as it is obtained from heating a substance in a gaseous, inert state, which at a certain temperature has its molecular bonds overcome,thus generating ions, which are accelerated and then made electrostatically stable after coming into contact with the various electron beams. This energy originates from the quantum leap that takes place in the gas atom and generates a high specific impulse, even greater than those generated in chemical propulsion (Choueiri, 2003).

3.2 Types of Electric Devices

For aerospace propulsion, there are several technologies. In this case, in order to understand the objective of studying Hall thrusters, chemical and electrical propulsion will be highlighted and a performance comparison will be established, in order to offer an assessment of which thruster is more technically advantageous to be used (Choueiri, 2003).

3.2.1 Resistojet

Figure 3.1 show a resistojet and basic components to work, its operation takes place electrothermally, from the heating of a propellant inside a chamber, where it will be resistively heated and with that it will produce gases that will be expanded by a suitable nozzle, which provides for obtaining a specific impulse (Goebel, 2008).

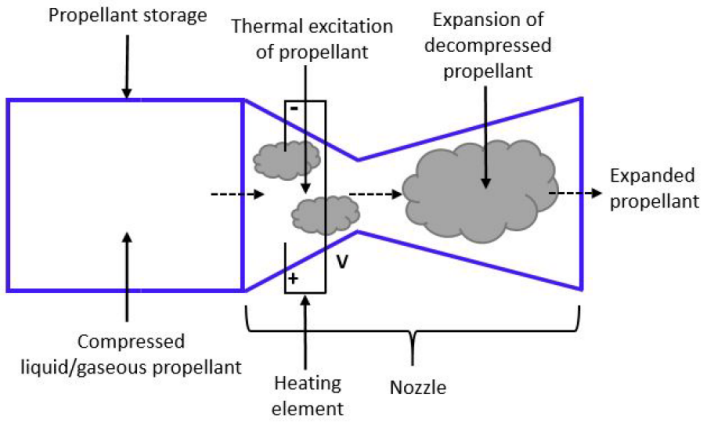

Figure 3.1. Schematic of a Resistojet. Source: (Tummala, 2017)

Resistojets have been used since 1965 on military satellites. Then commercial satellites were used and are currently used for orbit insertion, altitude control and satellite de-orbiting (Hoskins, 2013).

3.2.2 Arcjet

It has its operation, also known as electrothermal, through the transformation of a liquid propellant into a gaseous one with the use of an electric arc, which is produced from a high current, generating a spark and causing this obtaining of gases that are immediately directed in high velocity to the nozzle, thus generating thrust (Goebel, 2008). Figure 3.2 illustrates the schematic of an arcjet, highlighting components and operation.

They are considered to have low specific impulse, but they are used and, in general, have more specific uses to perform maneuvers on satellites to change direction. Hydrazine is generally used for this type of propellant (Hoskins, 2013).

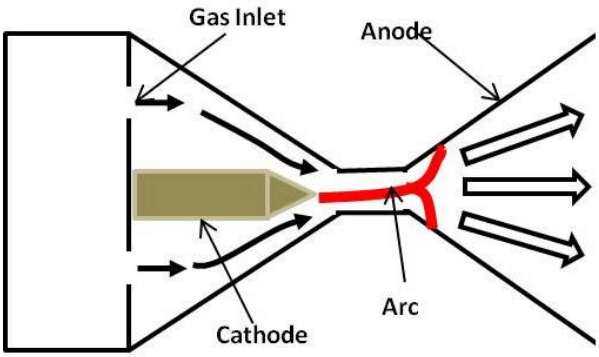

Figure 3.2. Schematic of an Arcjet. Source: (Yildiz *et al.*, 2015)

.

3.2.3 Ion Thruster

This type of system is already more evolved within electric propulsion. It is based on the ionization of certain propellants. The extracted ions are accelerated at high speeds at voltages in excess of 10 kV by electrostatic fields. The ionic thruster presents a superior performance to the other types of existing technologies in the electric propulsion, which in fact can be verified when analyzing that its efficiency is in the range of 60% to 80% (Goebel, 2008). Figure 3.3 represents an ion thruster using Xenon gas, illustrating key components.

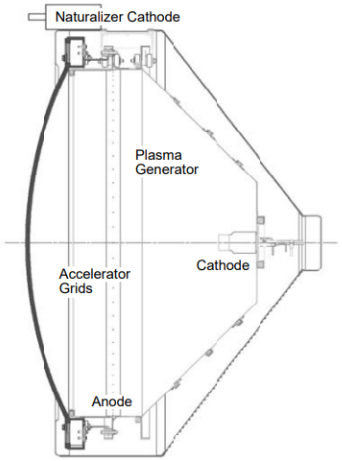

Figure 3.3. Schematic of an ionic propellant with Xenon gas. Source: (Goebel, 2008)

3.3 Hall Thruster and Cylindrical Hall Thruster

In electromagnetic propulsion we have the Hall thrusters, which are called like that, because this type of system has its operation based on the use of perpendicular discharges, $\mathbf{E} \times \mathbf{B}$, which produces the Hall current for plasma delivery. As show in figure 3.4 an electric and magnetic field set at a right angle accelerate ions to high speeds (Goebel, 2008).

The efficiency and specific impulse, in general, are below those obtained in the ion thruster,

but the thrust at a given power is greater and the construction of the model is simpler and requires less energy expenditure to maintain its operation. As a result, it is verified that its use is of relevant interest to the aerospace community because in addition to providing the reach of speeds and distances not yet explored, it has a better cost-benefit ratio (Goebel, 2008).

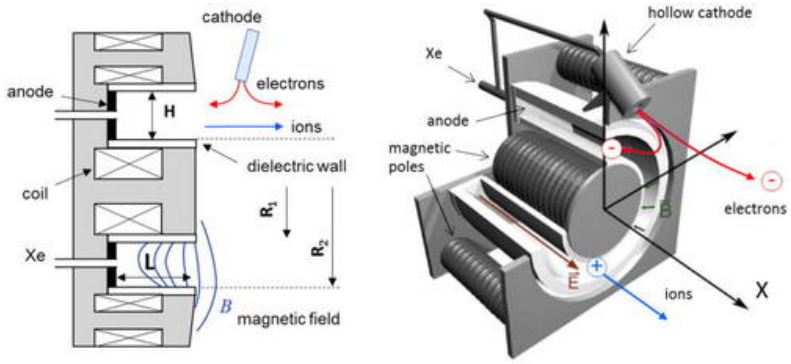

Figure 3.4. Schematic of a Hall thruster. Source: (Boeuf, 2017)

The possibility of its use in deep space exploration and also for orbital relocation maneuvers has been verified. The systems are sometimes combined and because they are so, at certain times they are used for one or more functions. See figure 3.5. This makes it possible to gain efficiency and precision in maneuvers and displacements (Choueiri, 2003).

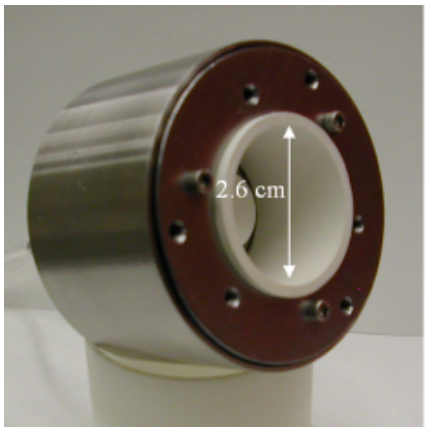

Figure 3.5. CHT thruster with SmCo permanent magnets. Source: (Raitses *et al.*, 2010)

Although the traditional Hall thrusters are used in space applications due to their reliability and efficiency, the development of the Cylindrical Hall Thruster (CHT) addresses specific challenges. The key distinction is in the discharge channel geometry. While the conventional Hall thrusters utilize an annular channel, the CHT adopts a cylindrical configuration, significantly reducing internal channel erosion issues and thereby enhancing durability and efficiency in long-duration missions.

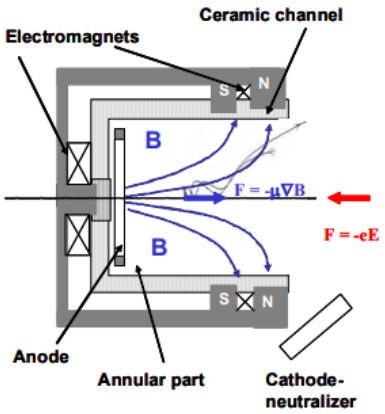

Figure 3.6. Schematic of Cylindrical Hall Thruster. Source: (Raitses *et al.*, 2010)

Therefore, the CHT is particularly advantageous for small-scale missions, such as CubeSats and microsatellites, where space and available power are limited. Its compact structure allows the system to maintain efficiency and functionality without straining limited resources. This adaptability amplify the range of applications for Hall thrusters, enabling their use in pioneering new frontiers of space exploration.

3.4 Plasma Physics Concepts

3.4.1 Criteria for Plasmas

Being distinct from solid, liquid, and gaseous states, a substance must meet specific criteria to be classified as plasma. For a gas to become plasma, a fraction of its atoms must be ionized, leading to the formation of free ions and electrons. According to Chen (2016), some aspects need be observed, such as:

1. Quasineutrality

Plasmas are quasineutral, meaning the ion density (n_i) and electron density (n_e) are approximately equal. While small deviations may occur locally, the overall neutrality is maintained when considering the plasma on a macroscopic scale. As stated by Chen (2016), plasma is a quasineutral gas of charged and neutral particles which exhibits collective behavior. This collective behavior refers not just to local interactions but also to the intrinsic nature of plasma, which involves electric and magnetic fields generated within itself (Chen, 2016).

2. Debye Length

To define quasineutrality more precisely, the system's physical dimensions (L) must be much larger than the Debye length (λ_D). In this context, according to Chen (2016):

- Debye shielding occurs when local concentrations of charge or external potentials are neutralized over a short distance (λ_D), leaving the bulk plasma largely free of significant electric fields or potentials.

- The Debye length represents the effective range of a charge's electric field before it is shielded by surrounding particles of opposite charge.
- If a charged particle is introduced into plasma, it will be surrounded by oppositely charged particles, which reduce its electric field, this phenomenon is known as shielding.
- The effective distance over which this shielding occurs is the Debye length (λ_D). Within this distance, the particle's electric field is significant; beyond it, the field is effectively canceled out by the arrangement of opposing charges. - This charge redistribution exemplifies the collective behavior characteristic of plasma.

The Debye length can be expressed as follows

$$\lambda_D = \sqrt{\frac{\varepsilon_0 k_B T_e}{n_e e^2}} \tag{3.1}$$

Where:
- ε_0: Permittivity of free space
- k_B: Boltzmann constant
- T_e: Electron temperature
- n_e: Electron number density
- e: Elementary charge

3. Debye Sphere Particle Number Criterion

The number of particles within a Debye sphere, known as the Debye number, must be much greater than 1. This ensures that collective effects dominate, an important property of plasma. The number of particles inside a Debye sphere can be represented by

$$N_D = n_e \frac{4}{3}\pi\lambda_D^3 \tag{3.2}$$

Where:
- N_D: Debye number
- n_e: Electron number density
- λ_D: Debye length

4. Ionization and Collisions

The degree of ionization and the dynamics of collisions also determine whether an ionized gas qualifies as plasma. A weakly ionized gas, such as a jet engine's exhaust, is not considered plasma because the charged particles frequently collide with neutral atoms. These collisions limit the particles' behavior to ordinary hydrodynamic forces rather than electromagnetic ones (Chen, 2016).

For a gas to behave as plasma, the condition $\omega\tau > 1$ must be met, where:

- ω is the frequency of typical plasma oscillations, and

- τ is the mean time between collisions with neutral atoms.

If this criterion is satisfied, electromagnetic forces dominate, allowing the gas to exhibit plasma behavior instead of behaving as a neutral gas. With this, Chen (2016) suggests that the three conditions a plasma must satisfy are:
1. $\lambda_D << L$
2. $N_D >>> 1$
3. $\omega\tau > 1$

3.5 DYNAMICS OF CHARGED PARTICLES IN ELECTROMAGNETIC FIELD

3.5.1 Uniform Magnetostatic Field

In this work, the analysis of particle dynamics is initially conducted using a uniform magnetic field to simplify the understanding of fundamental concepts. This approach serves as an introduction to the more complex scenario explored in the next section, where the interplay between magnetic and electric fields is analyzed. By starting with a uniform magnetic field, the focus remains on establishing a clear foundation, ensuring the subsequent analysis with electric fields builds upon well-defined principles.

For a uniform magnetic field, a solution in Cartesian coordinates system (x, y, z) can be obtained from the cross product between **v** and **B**, where $B = B\hat{z}$ (Bittencourt, 2004).

$$\mathbf{v} \times \mathbf{B} = \det \begin{vmatrix} \hat{x} & \hat{y} & \hat{z} \\ v_x & v_y & v_z \\ 0 & 0 & B \end{vmatrix} = B\left(v_y\hat{x} - v_x\hat{y}\right) \tag{3.3}$$

From the equation of motion, we have that

$$\frac{d\mathbf{v}}{dt} = \frac{qB}{m}\left(v_y\hat{x} - v_x\hat{y}\right) = \pm\Omega_c\left(v_y\hat{x} - v_x\hat{y}\right) \tag{3.4}$$

where Ω_c is known as cyclotron frequency (Bittencourt, 2004). The magnitude of the angular velocity is given by

$$\Omega_c = \frac{|q|B}{m} \tag{3.5}$$

For a positively charged particle $(q > 0)$ the Cartesian components of the velocity are

$$\frac{dv_x}{dt} = \Omega_c v_y \tag{3.6}$$

$$\frac{dv_y}{dt} = -\Omega_c v_x \tag{3.7}$$

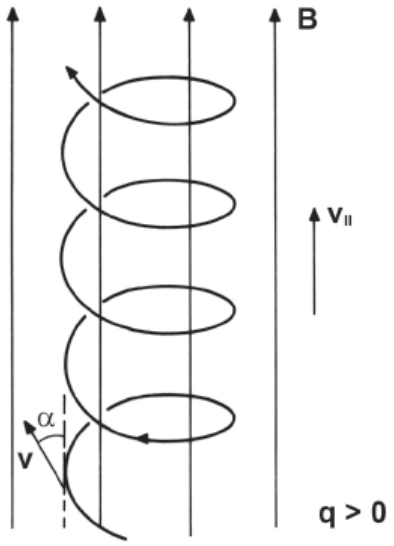

Figure 3.7. Helicoidal trajectory of a positively charged particle in a uniform magnetic field. Source: (Bittencourt, 2004)

$$\frac{dv_z}{dt} = 0 \tag{3.8}$$

since $v_z(t) = v_z(0) = v_{||}$ it means that there are no velocity changes along the Z axis. Therefore, if the initial velocity is zero, then the particle does not move in the Z axis. To obtain a solution for the velocity components perpendicular to the magnetic field, we take the derivative of (3.6) of both sides with respect to time (Bittencourt, 2004):

$$\frac{d^2v_x}{dt^2} = \Omega_c \frac{dv_y}{dt} \tag{3.9}$$

in the next step substitute the (3.7) to $-\Omega_c v_x$ and obtain

$$\frac{d^2v_x}{dt^2} = \Omega_c(-\Omega_c v_x) \tag{3.10}$$

then

$$\frac{d^2v_x}{dt^2} + \Omega_c^2 v_x = 0 \tag{3.11}$$

This results in a harmonic differential equation for v_x with solution

$$v_x(t) = v_\perp sin(\Omega_c t + \Theta_0) \tag{3.12}$$

Using an analogous analysis to determine $v_y(t)$, we obtain:

$$v_y(t) = v_\perp \cos(\Omega_c t + \theta_0) \tag{3.13}$$

Note that $v_\perp = \sqrt{v_x^2 + v_y^2}$. Therefore, now we have the velocity equations, and by integrating them, we obtain their positions, which are:

$$X_o = x_o + \frac{v_\perp}{\Omega_c} \cos(\theta_o) \tag{3.14}$$

$$Y_o = y_o - \frac{v_\perp}{\Omega_c} \sin(\theta_o) \tag{3.15}$$

Considering only a uniform magnetic field, it can be observed that the charged particle does not have displacement in the Z direction (Bittencourt, 2004).

3.5.2 Uniform Magnetostatic and Electrostatics Fields

In the following, we will review the dynamics of charged particles in the presence of electric **E** and magnetic **B** fields because their combination is the core of Hall thruster operation, including the cylindrical Hall thruster under study. These fields are fundamental to the propulsion mechanism itself.

The **E** $\times$ **B** configuration creates a drift that confines electrons enhancing ionization efficiency and enabling the generation of a plasma discharge that propels ions. This interaction can achieve the thrust required for spacecraft propulsion, Nanosatellites and Cubesats. Now, when considering the motion of charged particles with the application of both **E** and **B** fields, the particle will be accelerated or decelerated along the Z-axis, depending on the orientation of the field and the charge of the particle. Thus, the starting equation that correlates with the motion is:

$$m\frac{d\mathbf{v}}{dt} = q(\mathbf{E} + \mathbf{v} \times \mathbf{B}) \tag{3.16}$$

Using Cartesian coordinates, with the Z-axis in the direction of the magnetic field, in addition to the magnetic field in the Z direction, we have the electric field in all three directions as follows:

$$\mathbf{E} = E_x\hat{x} + E_y\hat{y} + E_z\hat{z} \tag{3.17}$$

With this, the equation of motion can be rewritten as.

$$\frac{d\mathbf{v}}{dt} = \frac{q}{m}[(E_x + v_y B)\hat{x} + (E_y - v_y B)\hat{y} + E_z\hat{z}] \tag{3.18}$$

For simplicity, we assume the particle has a positive charge. If the charge is negative, the results change by reversing the sign of Ω_c (Bittencourt, 2004).

The z component of this equation can be solved directly and corresponds to previously shown results. For the x and y components, differentiating dv_x/dt with respect to time and

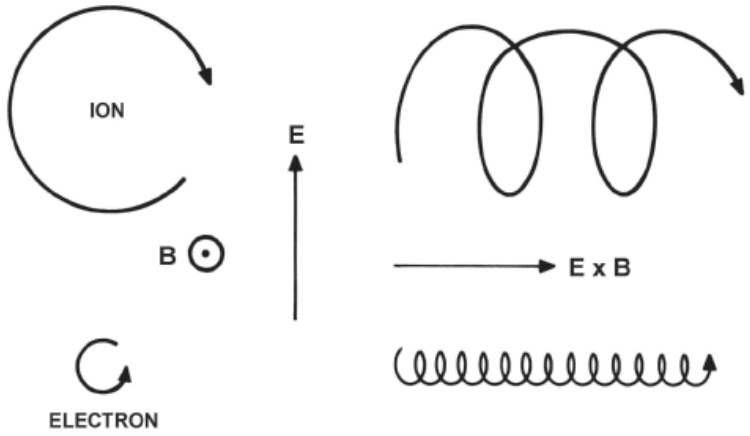

Figure 3.8. Cycloidal trajectories described by ions and electrons in crossed electric and magnetic fields. Source: (Bittencourt, 2004)

substituting dv_y/dt leads to:

$$\frac{d^2v_x}{dt^2} + \Omega_c^2 v_x = \Omega_c^2 \frac{E_y}{B}. \tag{3.19}$$

This is a non-homogeneous differential equation representing harmonic motion with a natural frequency Ω_c (Bittencourt, 2004). The general solution combines the homogeneous and particular solutions, yielding:

$$v_x(t) = v'_\perp \sin(\Omega_c t + \theta_0) + \frac{E_y}{B}, \tag{3.20}$$

where $v'_\perp$ and θ_0 are constants determined by initial conditions.

To obtain $v_y(t)$, substitute $v_x(t)$ into the equation of motion. This results in:

$$v_y(t) = v'_\perp \cos(\Omega_c t + \theta_0) - \frac{E_x}{B}. \tag{3.21}$$

The velocity components $v_x(t)$ and $v_y(t)$, which describe the motion in the plane perpendicular to the magnetic field $\vec{B}$, oscillate at the cyclotron frequency Ω_c with an amplitude $v'_\perp$. This oscillatory motion is combined with a constant drift velocity $\vec{V}_E$, given by:

$$\vec{V}_E = \frac{E_y}{B}\hat{x} - \frac{E_x}{B}\hat{y}. \tag{3.22}$$

This drift velocity corresponds to the case where $\vec{B} = B\hat{z}$.

By integrating the expressions for $v_x(t)$ and $v_y(t)$, the particle's trajectory in the (x,y) plane is:

$$x(t) = -\frac{v'_\perp}{\Omega_c} \cos(\Omega_c t + \theta_0) + \frac{E_y}{B} t + X_0, \tag{3.23}$$

$$y(t) = \frac{v'_\perp}{\Omega_c} \sin(\Omega_c t + \theta_0) - \frac{E_x}{B} t + Y_0, \tag{3.24}$$

where X_0 and Y_0 are constants determined by the initial conditions (Bittencourt, 2004).

$$X_0 = x_0 + \frac{v'_\perp}{\Omega_c} cos(\theta_0) \tag{3.25}$$

$$Y_0 = y_0 - \frac{v'_\perp}{\Omega_c} sin(\theta_0) \tag{3.26}$$

According to Bittencourt (2004), the motion of a charged particle in uniform electric and magnetic fields consists of three main components:

- **Acceleration along B:** The particle accelerates due to the electric field component $\boldsymbol{E}_\parallel$, with an acceleration of $\boldsymbol{qE}_\parallel/\boldsymbol{m}$. If $\boldsymbol{E}_\parallel = 0$, the particle's motion along $\boldsymbol{B}$ remains constant.
- **Cyclotron motion:** In the plane perpendicular to $\boldsymbol{B}$, the particle undergoes circular motion at the cyclotron frequency $\boldsymbol{\Omega_c} = \frac{|\boldsymbol{q}|\boldsymbol{B}}{\boldsymbol{m}}$, with a radius of $\boldsymbol{r_c} = \frac{\boldsymbol{v'_\perp}}{\boldsymbol{\Omega_c}}$.
- **Electromagnetic drift velocity:** The particle also moves with a constant drift velocity $\boldsymbol{V_E} = \frac{\boldsymbol{E}\times\boldsymbol{B}}{\boldsymbol{B}^2}$, which is perpendicular to both $\boldsymbol{B}$ and $\boldsymbol{E}$.

This are the physical principles that govern Hall thrusters and how they are applied to optimize performance in the cylindrical Hall thruster.

4 METHODOLOGY

4.1 NUMERICAL TOOLS

4.1.1 Finite Element Methods Magnetics - FEMM

Finite Element Method Magnetics (FEMM) is an advanced software tool designed to solve electromagnetic problems using the finite element method. This software is particularly useful for analyzing 2D planar and axisymmetric problems in electromagnetism. Developed by David Meeker, FEMM is open-source and widely used in academic research, engineering, and various industrial applications due to its powerful features and ease of use. FEMM addresses certain limiting cases of Maxwell's equations. The magnetic problems it tackles are classified as low frequency problems, where displacement currents can be disregarded (Meeker, 2015).

FEMM consists of three primary components: a preprocessor, a solver, and a postprocessor. The preprocessor enables users to create and modify the model's geometry, define material properties, and set boundary conditions. It provides an intuitive graphical interface where users can draw geometries or import them from other CAD programs. Moreover, FEMM supports the definition of complex material properties, including nonlinear materials, making it suitable for a broad range of magnetic and electric field simulations (Meeker, 2015).

The solver is the core of FEMM, where the finite element method is applied to solve the Maxwell's equations governing the electromagnetic fields. Users can specify different types of analyses, such as magnetostatic, time-harmonic magnetic, and electrostatic problems. FEMM's solver is known for its robustness and capability to handle large and complex models (Meeker, 2015).

The postprocessor enables users to visualize and analyze the results. It offers various tools to analysis the magnetic field distribution, flux density, force calculations, and other parameters. The users can generate plots and export data. Additionally, the post processor supports scripting, automating repetitive tasks, and customization of the analysis process (Meeker, 2015).

FEMM's versatility and user-friendly interface make it an excellent choice for engineers and researchers involved in electromagnetic design and analysis. Its capability to manage complex geometries and material properties, along with its open-source nature, allows for extensive customization and integration into larger simulation workflows. Whether designing electric motors, transformers, or other electromagnetic devices, FEMM offers a reliable and efficient solution for electromagnetic field analysis.

4.1.2 Hall Ion Sources - HALLIS

The Hallis software, Hall Ion Sources simulations software, specifically designed for Hall Effect Thrusters (HET), is a important tool in electric propulsion. Hall Effect Thrusters are utilized in space missions due to their efficiency and capacity to deliver continuous and controlled thrust over extended periods. The Hallis software tool simulates the physical and chemical processes occurring within a Hall thruster.

Hallis is a 2D hybrid model where electrons are treated as a fluid and ions and neutral atoms are represented by pseudoparticles. Users can select either the 1D or 2D model at the start of the simulation, and both models can be accessed and simulated for a same configuration of geometry (Laplace, 2018).

4.1.2.1 Introduction to the Hybrid Model and Fluid Description of Particles

The approximation made in the hybrid model for electrons, ions, and neutral atoms simplifies the description. This approach is used due to the high mobility of electrons and the slower dynamics of ions, which justifies their distinct treatment. The theoretical basis of this description is founded on the Boltzmann Equation, which defines the evolution of the distribution function $f(\mathbf{r}, \mathbf{v}, t)$ representing particle density in phase space given by Equation (4.1) (Taccogna e Garrigues, 2019).

$$\frac{\partial f}{\partial t} + \mathbf{v} \cdot \frac{\partial f}{\partial \mathbf{r}} + \frac{\mathbf{F}}{m} \cdot \frac{\partial f}{\partial \mathbf{v}} = \left\{ \frac{\partial f}{\partial t} \right\}_c \tag{4.1}$$

In this equation:

- The left-hand terms represent changes in the distribution due to time, position, and external forces ($\mathbf{F}$).
- The right-hand term represents changes due to collisions.

The transition from the kinetic model to the fluid description is achieved by integrating f over velocity space, resulting in the following macroscopic properties:

- **Density (n)**:
$$n = \int f(\mathbf{r}, \mathbf{v}, t) d^3v \tag{4.2}$$
Represents the number of particles per unit volume.
- **Velocity ($\mathbf{u}$)**:
$$\mathbf{u} = \frac{1}{n} \int \mathbf{v} f(\mathbf{r}, \mathbf{v}, t) d^3v \tag{4.3}$$
Describes the collective motion of particles.
- **Energy (ε)**:
$$\varepsilon = \frac{m}{2en} \int v^2 f(\mathbf{r}, \mathbf{v}, t) d^3v \tag{4.4}$$

Is the average kinetic energy per particle.

These properties are then used in the transport equations, which describe the macroscopic behavior of the plasma.

4.1.2.2 Fundamental Transport Equations

1. Continuity Equation

According to Taccogna e Garrigues (2019) the continuity Equation (4.5) describes how the electron density changes over time and space, accounting for particle sources and losses within the system:

$$\frac{\partial n_e}{\partial t} + \nabla \cdot (\mathbf{n_e u_e}) = S_v + S_w \tag{4.5}$$

Here:

- n_e: Electron density.
- u_e: Electron velocity.
- S_v: Volume sources of particle generated.
- S_w: Wall losses due to recombination.

This equation ensures particle conservation in the plasma and is directly derived from the Boltzmann Equation by integrating f over velocity space Taccogna e Garrigues (2019).

2. Momentum Equation

In the work of Taccogna e Garrigues (2019) the momentum Equation (4.6) describes the motion of electrons under the influence of external forces (electric and magnetic fields), collisions, and pressure gradients:

$$\frac{\partial \mathbf{u_e}}{\partial t} + (\mathbf{u_e} \cdot \nabla)\mathbf{u_e} = \frac{e}{m_e}(\mathbf{E} + \mathbf{u_e} \times \mathbf{B}) - \frac{e}{m_e n_e}\nabla(n_e T_e) - \nu_e \mathbf{u_e} - \frac{S_w}{n_e}\mathbf{u_e} \tag{4.6}$$

Here:

- E: Electric field.
- B: Magnetic field.
- T_e: Electron temperature.
- ν_e: Electron collision frequency.

This equation is essential to model electron transport across the magnetic field ($\mathbf{E}+\mathbf{u_e}\times\mathbf{B}$) and the effects of collisions within the plasma.

3. Energy Equation

According to Taccogna e Garrigues (2019) the energy Equation (4.7) describes how the energy of electrons ($n_e\varepsilon_e$) evolves over time and space, taking into account the work done by fields, thermal transport, and energy losses:

$$\frac{\partial(n_e\varepsilon_e)}{\partial t} + \nabla\cdot(n_e\varepsilon_e\mathbf{u_e} + \mathbf{P_e}\cdot\mathbf{u_e} + \mathbf{Q_e}) = -en_e\mathbf{u_e}\cdot\mathbf{E} - C_{e,v} - C_{e,w} \tag{4.7}$$

Here:

- P_e: Electron pressure.
- Q_e: Heat flux associated with temperature gradients.
- $-en_e\mathbf{u_e}\cdot\mathbf{E}$: Energy loss due to work done by the electric field.
- $C_{e,v}$: Collisional losses by electrons.
- $C_{e,w}$: Energy losses at the walls.

These three equations are applied to electrons, which are treated as a fluid. On the other hand, ions and neutral atoms are treated as pseudo-particles to simulate kinetic processes such as ionization and recombination.

The reason for using these equations in the hybrid model is their ability to offer a simplified yet accurate description of the collective behavior of electrons. This reduces computational complexity while still capturing key phenomena like cross-field transport, pressure gradients, and energy losses.

4.2 PHYSICS DESCRIBED BY HALLIS

4.2.1 Electron Mobility

The mobility of electrons in magnetized plasmas follows classical collisional transport theory and is expressed as Equations (4.8) and (4.9) (Laplace, 2018):

1. **Parallel Mobility ($\mu_\parallel$)**

$$\mu_\parallel = \frac{e}{m}\frac{\Omega_{ce}}{\nu^2+\Omega_{ce}^2} \tag{4.8}$$

where ν is the electron collision frequency as can be seen in the Equation (4.11).

2. **Perpendicular Mobility ($\mu_\perp$)**

$$\mu_\perp = \frac{e}{m}\frac{\nu}{\nu^2 + \Omega_{ce}^2} \tag{4.9}$$

where $\Omega_{ce} = \frac{eB}{m_e}$ is the electron cyclotron frequency.

3. **Hall Parameter (H)** The ratio of parallel to perpendicular mobility is given by the Hall parameter:

$$H = \frac{\mu_\parallel}{\mu_\perp} = \frac{\Omega_{ce}}{\nu}. \tag{4.10}$$

The Hall parameter can reach very high values (greater than 10^3) in the exhaust region if the collision frequency only accounts for electron-neutral and electron-ion Coulomb collisions (Laplace, 2018).

4. **Effective Electron Collision Frequency (ν)**

The effective electron collision frequency in the HALLIS model accounts for multiple contributions (Boeuf, 2017):

$$\nu = \nu_{en} + \nu_c + \nu_{\text{Bohm}} + \nu_{\text{Wall}}, \tag{4.11}$$

where:

- ν_{en}: Electron-neutral collision frequency,
- ν_c: Electron-Ion coulomb collision frequency,
- ν_{Bohm}: Effects of instabilities and turbulence transport,
- ν_{Wall}: Effects of electron-wall collisions.

4.2.2 Ion Transport

In fluid models, the ion continuity and momentum equations are solved at each time step using the electric field E and ionization rate according to Equation (4.12) (Laplace, 2018).

$$S = n_e n_a k_i(T_e) \tag{4.12}$$

Here, S represents the rate of ion production and $k_i(T_e)$ is the ionization rate that depends on the electron temperature. Assuming the principle of quasineutrality, where the electron density n_e is equal to the ion density n_i, we can express the plasma density as $n = n_e = n_i$. Additionally, n_a represents the atom density Laplace (2018). In hybrid models, ions are treated as particles, moving according to the electric field and accounting for ionization and wall losses. By the end of the time step, the plasma density n and ion flux Equation (4.13) are determined by:

$$\Gamma_i = n v_i \tag{4.13}$$

4.2.3 Electron Temperature

Using the plasma density and electric field as initial inputs, and assuming the electron flux follows a drift-diffusion model, the electron temperature at the next time step is determined by integrating the electron energy equation. This calculation assumes a Maxwellian distribution for electrons and neglects drift energy compared to thermal energy (Laplace, 2018):

$$\frac{3}{2}\frac{\partial(nT_e)}{\partial t} + \frac{5}{2}\nabla\cdot(\Gamma_e T_e) - \frac{5}{2}\nabla\cdot(\mu_e n T_e \nabla T_e) = -\mathbf{E}\cdot\Gamma_e - n_a n\kappa - nW \tag{4.14}$$

In this equation:

- $\kappa = \varepsilon\nu_{\varepsilon w}$: Represents the energy loss rate due to electron-atom collisions, derived from cross-sections and electron temperature.
- $W = \varepsilon\nu_{\varepsilon}$: Accounts for energy losses caused by interactions with the channel walls.
- μ_e: Is the electron mobility

The relations between Electron Temperature and Energy is

$$\varepsilon : \frac{3}{2}k_B T_e \tag{4.15}$$

Where ε is the energy of the electrons. The software HALLIS directly displays the electron energy, rather than the electron temperature itself (Laplace, 2018).

4.2.4 Neutral atom transport

In the context of neutral atom transport, atoms are released from the channel's end following a semi-Maxwellian flux distribution. For a gas temperature T_a, their average axial velocity is given by Equation (4.16) (Laplace, 2018):

$$\bar{v}_z = \sqrt{\frac{\pi}{2}}v_T \tag{4.16}$$

Where,

$$v_T = \sqrt{\frac{2k_B T_a}{M}} \tag{4.17}$$

In this equation:

- $\bar{v}_z$: Is the average axial velocity of the emitted atoms.
- v_T: Represents the thermal velocity of the atoms, which is determined by their temperature and mass.

- k_B: Is the Boltzmann constant, which relates the thermal energy of particles to their temperature.
- T_a: Is the temperature of the gas, influencing the thermal energy of the emitted atoms.
- M: Is the mass of the atom, affecting its velocity for a given thermal energy.

Atoms can also form at the walls (sides or channel end) through ion recombination. It is generally assumed that these atoms are emitted at the gas-wall temperature T_a with a semi-Maxwellian distribution (Laplace, 2018).

4.2.4.1 Features of Hallis Software

1. Plasma Simulation: Hallis offers modeling of the plasma dynamics within the thruster. to analyze the behavior of ions and electrons under the influence of magnetic and electric fields, providing insights into plasma density, temperature and potential distributions.

2. Magnetic Field Analysis: The software includes advanced modules for analyzing the magnetic field configurations. This is important because the magnetic field occupies a significant role in confining and accelerating the plasma, directly impacting the thruster's performance.

3. Ionization and Collision Processes: Hallis simulates the ionization process, where neutral atoms are transformed into ions, with various collision processes, including interactions between electrons and neutrals, ions and neutrals, and between ions themselves. These processes are essential for understanding energy transfer mechanisms and optimizing thruster efficiency.

4. Thermal and Structural Analysis: The software include thermal analysis tools to predict temperature distributions within the thruster components. This helps in designing thrusters that can withstand the extreme thermal environments encountered during operation.

5. User-Friendly Interface: Hallis is designed with a user-friendly interface. It includes visualization tools for interpreting simulation results, which aids in the process of design and optimization. Researchers with less experience with the software don't have difficulties using the software.

4.2.5 Applications in Space Propulsion

Hall Thrusters are essential for present space missions, particularly, in scenarios requiring precise spacecraft trajectory control, such as satellite station keeping, interplanetary missions, and orbital transfers. Hallis software optimizes thruster design, analyzing performance and reliability for space missions.

By offering a detailed insight into the physical processes within the thruster, Hallis facilitates the design of more efficient and durable propulsion systems. This takes to reduced fuel

consumption, longer mission durations, and enhanced mission capabilities, making Hallis a valuable tool in aerospace engineering.

Therefore, Hallis is a excellent software for modeling and optimizing Hall Thrusters. Its advanced simulation features, combined with a user-friendly interface, make it an important resource for researchers and engineers working on electric propulsion systems. As space exploration progresses, tools like Hallis will be pivotal in advancing the boundaries of space missions.

4.3 Baseline Geometry

The baseline geometry, figure 4.1, utilized in this study is based on the work by Rodrigo A. Miranda, Alexandre A. Martins, and José L. Ferreira, titled "Particle-in-Cell Numerical Simulations of a Cylindrical Hall Thruster with Permanent Magnets" (DOI: 10.1088/1742-6596/911/1/012021). The figure presented illustrates the essential geometric components of the Cylindrical Hall Thruster (CHT), offering a clear depiction of the structure and functionality of the system.

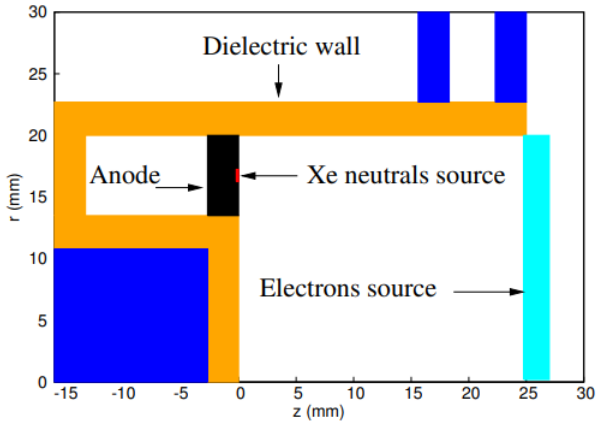

Figure 4.1. Simulation domain representing the upper-half cross-section of a Cylindrical Hall Thruster. Source: (Miranda *et al.*, 2017)

- Anode: In black, the anode serves as the injection point for neutral xenon gas, which is essential for the the ionization process within the thruster.
- Xe Neutrals Source: Located adjacent to the anode (small red region), this region marks where neutral xenon atoms are introduced into the channel for subsequent ionization.
- Dielectric Wall: The yellow colored dielectric wall plays a role in plasma confinement, ensuring that charged particles interact effectively within the cylindrical channel and minimizing energy losses.
- Electrons Source: Shown on the right, in the cyan region, this source provides the electrons required to ionize the neutral xenon gas, emulating the function of the cathode in a real Hall thruster.

- Magnetic Regions: The blue regions at the boundaries represent the permanent magnets.

This geometry facilitates the investigation of physical phenomena such as magnetic confinement, electron transport, and ion acceleration efficiency which are fundamental to the operation of a Cylindrical Hall Thruster. Furthermore, employing this configuration ensures consistency with the existing literature and establishes a robust foundation for validating the obtained results.

4.4 Simulation Setup

We employ the Finite Element Method Magnetics (FEMM) software to compute the magnetic field due to the permanent magnets. The simulations were performed in a two dimensional (2D) domain, keeping the axial and radial directions, and ignoring variations in the azimuthal direction. Figure 4.3 shows the simulation domain defined in the FEMM software. The vertical axis corresponds to the axial direction, and the geometry is symmetric around this axis.

The axis transposition was necessary to implement in the FEEM, adjusting the coordinate system representations for an appropriate visualization of the radial and axial component relationships, according to the figure 4.2.

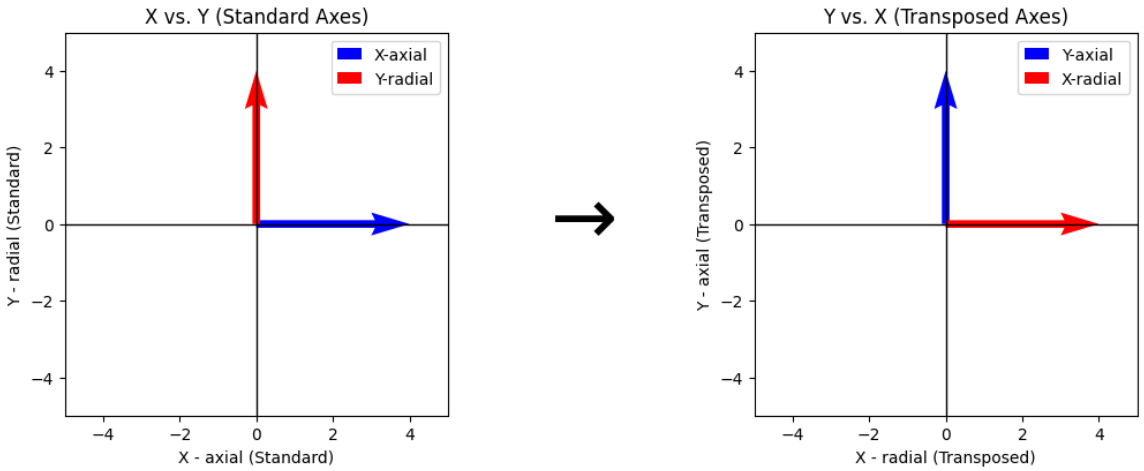

Figure 4.2. Visualization of Axis Transposition for Radial and Axial Component Representation.

The position of the samarium-cobalt magnets are indicated by rectangles labeled by SmCo36, and their polarization is indicated by a small arrow, note in 4.3. The regions marked as “Air” represent empty space. The contours between adjacent “Air” regions are defined for controlling the number of finite elements inside each region, and do not represent solid boundaries. The boundary of the simulation domain has a semicircular shape, and is set to Dirichlet conditions.

For the simulation of the plasma inside the channel, we use the Hall Ion Sources Simulation Software (HALLIS) which is a hybrid code developed at the LAPLACE laboratory (Laplace, 2018). The HALLIS software includes two autonomous modules for performing 1D e and 2D

simulations, using a hybrid model for the plasma. In this model, electrons are treated as a fluid and neutral atoms are represented by pseudo-particles (Hagelaar *et al.*, 2002).

The simulations start by injecting xenon neutral gas into the cylindrical chamber, resulting in a distribution density of neutrals inside the channel. The trajectories of positive ions and neutral atoms are computed through the integration of the equations of motion, considering collisions and interactions with walls (specular or diffusive). The transport of electrons across the magnetic barrier is described by empirical coefficients for the effective mobility and energy losses. In this work, were examine two different values of the electric potential, namely, 150V and 300V.

Table 5.1 shows the numerical values of the simulation parameters of the HALLIS software. For each value of the anode potential, simulation results were recorded at three time, $t1$ = 450 μs , $t2$ = 500 μs , $t3$ = 550 μs. After obtaining the analyzed data for each moment, an average was calculated for a better visualization of the results.

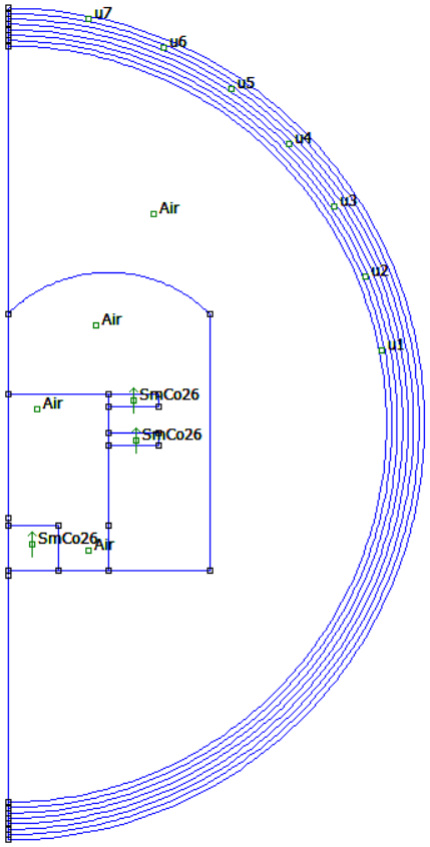

Figure 4.3. Simulation domain defined in the FEMM software, showing the position of the permanent magnets, marked as “SmCo36”.

5 RESULTS

5.0.1 Magnetic Field Simulations

We start by computing the magnetic field due to the presence of permanent magnets in a CHT using the FEMM software. The default installation of the HALLIS software offers example simulation files for a SPT-100 Hall thruster. Since the geometry of a CHT is different from the SPT-100 thruster, there was the necessity to create a custom simulation file in FEMM representing the geometry and position of the permanent magnets of a CHT. Some trial-and-error was needed to obtain the correct simulation file in FEMM, and import the results to the HALLIS sofware, because the HALLIS software applies a set of linear transforms (such as translations, rotations and scaling) on the imported files from FEMM. Since the documentation was not very clear about these transformations, several tries were needed until the results from FEMM were correctly imported in HALLIS.

Figure 5.1 shows the grid of finite elements needed for the calculation of the magnetic field due to the permanent magnets. From this figure it is verified that the number of elements increase at the boundaries of the simulation domain, resulting in a finer grid at these boundaries. Figure 5.2 shows the resulting magnetic field lines, which extend from the positions of the permanent magnets, and their shapes depend on the polarization as defined in Fig. 4.3. The intensity of the magnetic field is represented by a color scale, where the blue color indicates minimum values and the red color indicates maximum values. Clearly, the maximum values of the magnetic field strength are located inside the permanent magnets and decreases with the distance from the magnets, which is expected.

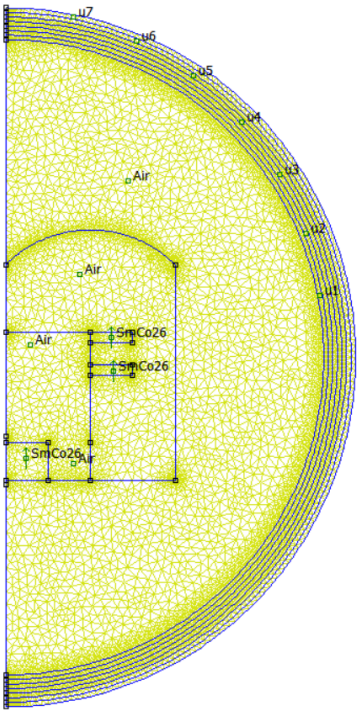

Figure 5.1. Mesh used by FEMM with 11814 nodes.

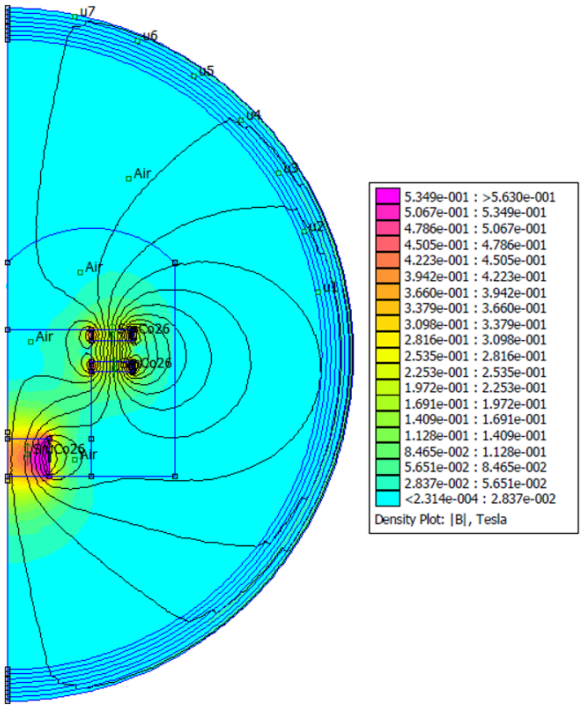

Figure 5.2. The resulting magnetic field, and magnetic field lines. Note that the horizontal axis represents the radial direction, and the vertical axis represents the axial direction of the cylindrical coordinates.

Table 5.1. Numerical values of the simulation parameters with the HALLIS software.

Parameters	Values (cm)
Axial domain	5.00
Radial domain	2.50
Channel Lenght	2.50
Inner Radius	0.00
Outer Radius	2.00
Cathode position	(2.50, 1.00)
Anode	(0.00 , 1.50)
Gas inlet	(1.25, 1.75)
Gas flow rate	5.0 mg/s
Gas temperature	500 K

5.0.2 Plasma simulations

In this section we compute the resulting plasma density, electric potential and electron energy using two values of the electrostatic potential at the anode, namely, 150 V and 300 V. The magnetic field computed using the FEMM software and imported into the HALLIS software is depicted in Figure 5.3. Note that the HALLIS software defines the cylindrical coordinate system in a different manner compared to the FEMM software. In the FEMM software, the horizontal axis represents the radial direction, whereas the vertical axis represents the axial direction, whereas in the HALLIS software, the horizontal axis represents the axial direction and the vertical axis represents the radial direction. Since the magnetic field model in FEMM has been modified to represent the CHT configuration, it is important to verify that the magnetic field from FEMM has been imported correctly to HALLIS. The modulus of the magnetic field is represented in a color scale, and displays variations in the axial (X) and radial (Y) directions of the channel. Note that the field lines concentrate closer to the location of the permanent magnets, which is also a region with higher magnetic field strength.

Figure 5.4 shows the results for an anode potential of 150 V. The electrostatic potential has a maximum value near the anode and decreases rapidly in the axial direction toward the channel exit region. The plasma density displays large values near the $Y = 0$ central axis of the channel. However, a localized maximum can be also distinguished towards the anode. This isolated maximum is due to a population of electrons trapped by the magnetic field, and colliding with the neutral gas, causing an enhancement of ionization and higher plasma density values.

Following that, the anode potential was adjusted to a value of 300 V keeping all other parameters fixed. Figure 5.5(a) shows that the electrostatic potential displays a similar pattern with the 150 V case. However, a narrow strip of low values extending from the anode to the channel exit can be observed.The plasma density also indicates the presence of a narrow strip linking the anode region to the central region at the channel exit, where the highest values are observed. Evidently, the higher potential value at the anode can increase the ionization rate near the anode, due to a higher number of electrons trapped in that region where the magnetic field is stronger (see Fig. 5.3).

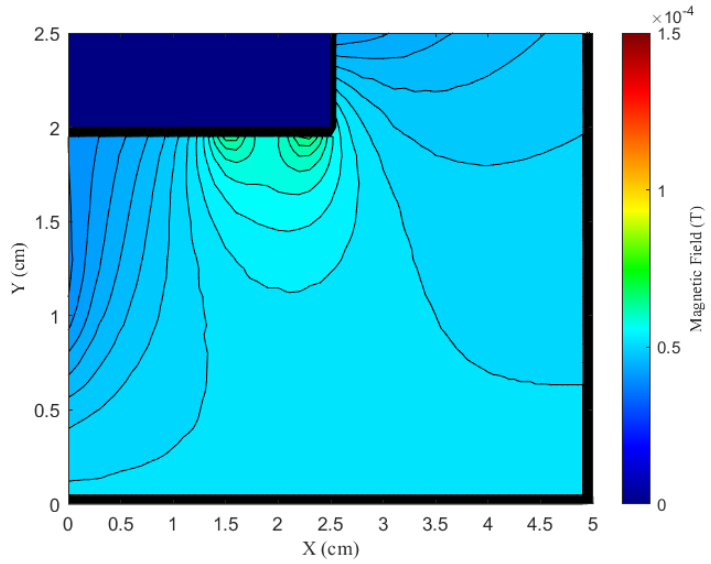

Figure 5.3. The magnetic field lines and the modulus of the magnetic field in color scale in the HALLIS software. Note that the horizontal axis represents the axial direction, and the vertical axis represents the radial direction.

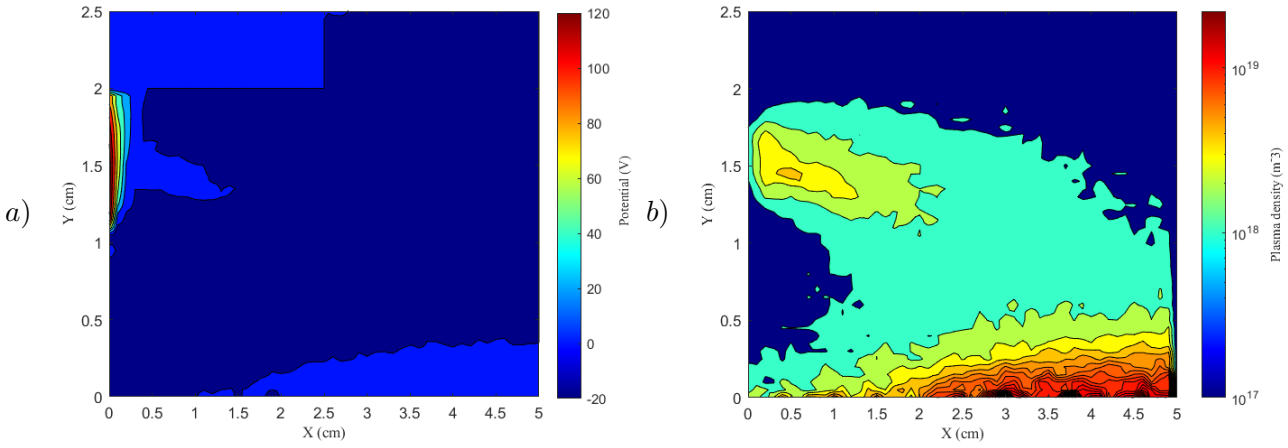

Figure 5.4. Contour plots of (a) the electrostatic potential, and (b) plasma density, for 150 V.

The Figure 5.6 compares the distribution of electron energy in a CHT operating at different anode potentials. The first image 5.6(a), with a 150 V potential, the electron energy is concentrated in a region close to the anode, indicating limited ionization and confinement. It is worth noting that at 150 V, the electron energy oscillates around 25 eV, whereas at 300 V, it reaches approximately 50 eV, reflecting a significant increase in energy levels. The second image 5.6(b), corresponding to 300 V, reveals more intense energy distribution across the discharge channel. This suggests enhanced ionization efficiency and higher energy electrons due to the stronger electric field. While the 300 V potential enables improved performance metrics such as thrust and specific impulse, it also requires more power, which can challenge energy restrictions in CubeSats and small satellites. Thus, the 150 V operation favors power efficiency, while the 300 V operation enhances propulsion effectiveness, reflecting a trade-off between power consumption and performance optimization.

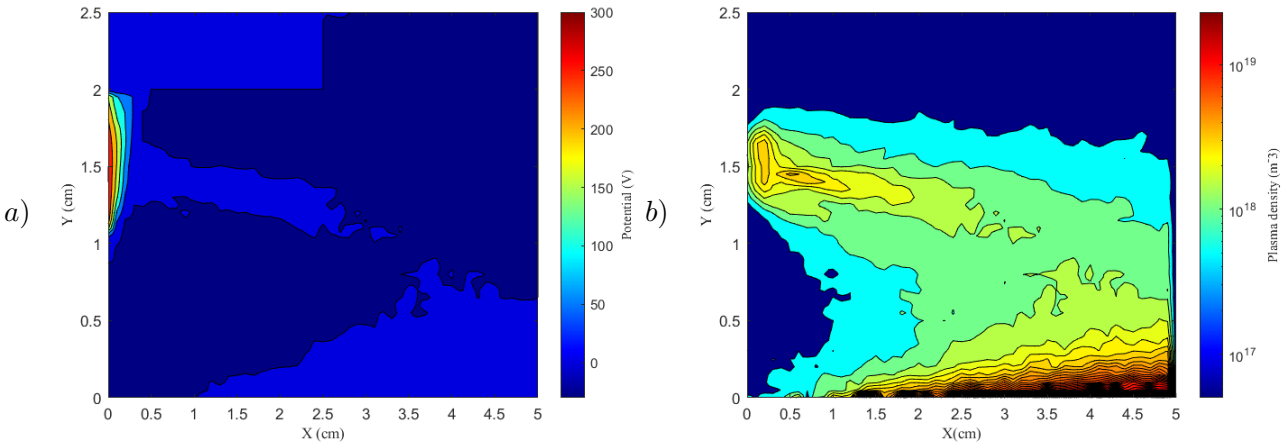

Figure 5.5. Contour plots of (a) the electrostatic potential, and (b) plasma density, for 300 V.

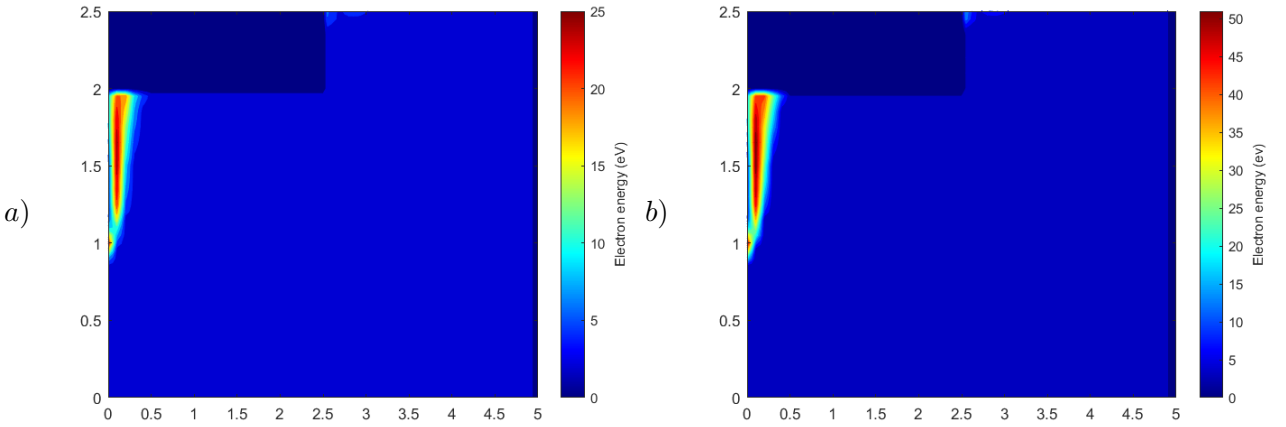

Figure 5.6. Contour plots of (a) the electron energy for 150v, and (b) electron energy for 300 V.

The performance of plasma thrusters can be evaluated by operational parameters such as thrust, specific impulse (I_{sp}), and efficiency (η). The thrust in this type of propulsion systems has units of millinewtons and can be written by Equation (5.1):

$$T = -v_{ex}\dot{m}_p \tag{5.1}$$

where m_p is the mass of propellant, $\dot{m}_p$ represents the mass variation in time, and v_{ex} is the exhaust velocity.

The specific impulse is defined by Equation (5.2):

$$Isp = \frac{T}{\dot{m}g} \tag{5.2}$$

where $\dot{m}$ is the xenon mass flow rate. Thus, the Tables 5.2 and 5.3 shows the values of these parameters for 150 V, and 300 V.

The efficiency of the thruster is given by

$$\eta_R = \frac{1}{2}\frac{T^2}{\dot{m}P} \tag{5.3}$$

where P is the power. In this equation the thrust is in units of mN, and the power is in units of KW. Equation 5.3 describes the proportion of the input propellant mass that is converted into ions and subsequently accelerates within the electric thruster.

The efficiency can be also computed by

$$\eta_A = \eta_u \cdot \eta_c \cdot \eta_E \tag{5.4}$$

where η_u is the efficiency of the propellant, given by

$$\eta_u = \frac{\text{extracted ion current}}{\text{ion current}} = \frac{I_i}{I_a} \tag{5.5}$$

where $I_a = \frac{\dot{m}}{m}$, η_c is the current efficiency defined by

$$\eta_c = \frac{\text{extracted ion current}}{\text{total discharge current}} = \frac{I_i}{I_T}, \tag{5.6}$$

and η_E is the energy efficiency is given by

$$\eta_{\mathrm{E}} = \frac{m_a \langle v \cos\theta \rangle^2}{2eV} \tag{5.7}$$

In a steady-state condition, these two efficiency analysis methods (η_R,η_A) should exhibit similar values (Laplace, 2018).

Tables 5.2 and 5.3 show the numerical values of the performance parameters obtained for 150 V and 300 V, respectively. It is clear that all parameters are higher for the higher anode voltage. However, the power also increases, which is an important issue for small satellites in which there is limited power available.

Table 5.2. Performance parameters for 150 V.

Performance at 150 V	
Parameters	**CHT Values**
Thrust (mN)	21.250
Specific Impulse (s)	433.23
Power (W)	254.768
Efficiency (η_R)	17.9
Efficiency (η_A)	23.8

Table 5.3. Performance parameters for 300 V.

Performance at 300V	
Parameters	**CHT Values**
Thrust (mN)	46.012
Specific Impulse (s)	938.07
Power (W)	715.616
Efficiency (η_R)	30.1
Efficiency (η_A)	32.7

6 CONCLUSIONS

In this work we performed numerical simulations of a cylindrical Hall thruster, which is an electric propulsion device for CubeSats, when compared to traditional Hall Thrusters, due to its smaller dimensions, and is designed specifically to operate at low power levels. Its geometry reduces susceptibility to channel wall erosion and makes it particularly suitable for low-power operations ($< 200W$) (Garrigues *et al.*, 2008).

We compare the operational parameters of this thruster for two different values of the electrostatic potential at the anode, namely, 150 V and 300 V. Our numerical results indicate that the potential drop is primarily concentrated in the cylindrical section of the channel and into the plume. Two peaks in plasma density were observed: one in the annular region and the other at the axis further to the exit thruster $(x > 2.5cm)$, which is attributed to the converging ion flux.

The efficiencies η_R and η_A showed proximity in the results. The first simulation (150V) exhibited a difference of 25%; however, for the second simulation (300V), there was a difference of 8%. These discrepancies are related to the averaging process during computation (Laplace, 2018).

The performance of the CHT at 300 V displays higher values compared to the 150 V case. However, the power needed for the thruster also increases. The energy available at small satellites, and in CubeSats in particular, is very limited. Using permanent magnets for the generation of the magnetic field can reduce the power requirements of the CHT to the range of 50 - 300 W, compatible with that available for CubeSats. Since the power required for the 300 V configuration is outside this range, further work is needed to reduce the power needed while increasing the potential at the anode. Nevertheless, the analysis presented in this work can be useful to decide which configuration is the most adequate, taking into account the power available of the propulsion system from a satellite power system.

The results obtained in this study show significant similarities with those presented by Garrigues *et al.* (2008). in their simulations of a miniaturized Cylindrical Hall Thruster (micro-CHT). Similar to Garrigues' work, the potential distributions highlight a concentration of the potential drop in the cylindrical region of the channel and exhibit comparable plasma density patterns.

7 PUBLICATIONS RELATED TO THIS WORK

7.1 PUBLISHED ARTICLES

- Comparison of the performance of a cylindrical Hall thruster with different anode voltages via numerical simulations. Published in Mathematics in Engineering and Aerospace (MESA).
- Comparison of the performance of a cylindrical Hall thruster with different anode voltages via numerical simulations. Presented at the Congress on Computational Methods in Engineering (CILAMCE 2024).
- Numerical Simulations of a Plasma Thruster for CubeSats. Presented at the National Congress of Mechanical Engineering Students (CREEM 2024).
- Particle-in-Cell Numerical Simulations of Plasma Particles in a Cylindrical Hall Thruster. Presented at the IV Conference on Dynamics, Control, and Applications to Applied Engineering and Life Sciences (DYCAELS 2023).
- Numerical Simulations of Plasma Particles in a Cylindrical Hall Thruster. Published at the Brazilian Colloquium on Orbital Dynamics (CBDO 2022).

REFERENCE LIST

Bittencourt, J. A. (2004). *Fundamentals of Plasma Physics*. Springer, Berlin.

Boeuf, J.-P. (2017). Tutorial: Physics and modeling of hall thrusters. *Journal of Applied Physics*, 121(1):011101.

Chen, F. F. (2016). *Introduction to Plasma Physics and Controlled Fusion*. Springer International Publishing, Cham, Switzerland, 3rd edição.

Choueiri, E. Y. (2003). Electric propulsion. In *Encyclopedia of Physical Science and Technology*, páginas 125–141. Elsevier.

Garrigues, L., Hagelaar, G., Boeuf, J., Raitses, Y., Smirnov, A., e Fisch, N. (2008). Simulations of a miniaturized cylindrical hall thruster. *IEEE Transactions on Plasma Science*, 36(5):2034–2042.

Goebel, D. M. (2008). *Fundamentals os Eletric Propulsion: Ion and Hall Thrusters*. New Jersey: John Wiley & Sons.

Hagelaar, G. J. M., Bareilles, J., Garrigues, L., e Boeuf, J. P. (2002). Two-dimensional model of a stationary plasma thruster. *Journal of Applied Physics*, 91(9):5592–5598.

Hoskins, W. A. (2013). 30 years of electric propulsion flight experience at aerojet rocktdyne. *Journal of Mechanisms and Robotics*.

Laplace, I. (2018). Hybrid model of hall ion sources, user´s manual. https://www.hallis-model.com/.

Meeker, D. (2015). Finite element method magnetics, user's manual. http://www.femm.info/Archives/doc/manual42.pdf.

Miranda, R. A., Martins, A. A., e Ferreira, J. L. (2017). Particle-in-cell numerical simulations of a cylindrical hall thruster with permanent magnets. *Journal of Physics: Conference Series*, 911:012021.

Raitses, Y. e Fisch, N. (2001). Parametric investigations of a nonconventional hall thruster. *Physics of Plasmas*, 8(5):2579–2586.

Raitses, Y., Gayoso, J. C., Merino, E., e Fisch, N. J. (2010). Effect of the magnetic field on the plasma plume of the cylindrical hall thruster with permanent magnets. In *46th AIAA/ASME/SAE/ASEE Joint Propulsion Conference & Exhibit*, Nashville, TN. American Institute of Aeronautics and Astronautics.

Seo, M., Lee, J., Seon, J., June Lee, H., e Choe, W. (2013). Effect of the annular region on the performance of a cylindrical hall plasma thruster. *Physics of Plasmas*, 20(2):023507.

Taccogna, F. e Garrigues, L. (2019). Latest progress in hall thrusters plasma modelling. *Reviews of Modern Plasma Physics*, 3(1). Available at: `https://hal.science/hal-02326278/file/Taccogna_Garrigues%20%281%29.pdf`.

Tummala, Dutta, A. (2017). An overview of cube-satellite propulsion technologies and trends. *Aerospace*, 4(4).

Yildiz, M. S., Unal, A. N., Ozkan, O., Koc, I., e Celik, M. (2015). Electrothermal propulsion system selection for communication satellite NSSK maneuver using multi criteria decision making method. In *2015 7th International Conference on Recent Advances in Space Technologies (RAST)*. IEEE.